Three-dimensional Finite Element Analysis of the Effect of Alveolar Cleft Bone Graft on the Maxillofacial Biomechanical Stabilities of Unilateral Complete Cleft Lip and Palate

Tao Tian
West China School of Stomatology,Sichuan University
Han-yao Huang
West China School of Stomatology,Sichuan University
Wei Wang
Urumql DW Innovation InfoTech Co.,Ltd.
Bing Shi
West China School of Stomatology,Sichuan University
Qian Zheng (zq652@163.com)
Sichuan University
Cheng-hao Li
West China School of Stomatology,Sichuan University

Research

Keywords: Unilateral complete cleft lip and palate, Alveolar cleft bone graft, Maxillofacial bone, Maxillofacial bone suture, Equivalent stress, Equivalent strain

Posted Date: October 11th, 2021

DOI: https://doi.org/10.21203/rs.3.rs-948465/v1

Abstract

Background: The objective was to clarify the effect of alveolar cleft bone graft on maxillofacial biomechanical stabilities, the key areas when bone grafting and in which should be supplemented with bone graft once bone resorption occurred in UCCLP (Unilateral Complete Cleft Lip and Palate).

Methods: Maxillofacial CAD (Computer Aided Design) models of non-bone graft and full maxilla cleft, full alveolar cleft bone graft, bone graft in other sites of the alveolar cleft were acquired by processing the UCCLP maxillofacial CT data in three-dimensional modeling softwares. The maxillofacial bone equivalent (EQV) stresses and bone suture EQV strains under occlusal states were obtained in the finite element analysis software.

Results: Under corresponding occlusal states, the EQV stresses of maxilla, pterygoid process of sphenoid bone on the corresponding side and anterior alveolar arch on the non-cleft side were higher than other maxillofacial bones, the EQV strains of nasomaxillary, zygomaticomaxillary and pterygomaxillary suture on the corresponding side were higher than other maxillofacial bone sutures. The mean EQV strains of nasal raphe, the maximum EQV stresses of posterior alveolar arch on the non-cleft side, the mean and maximum EQV strains of nasomaxillary suture on the non-cleft side in full alveolar cleft bone graft model were all significantly lower than those in non-bone graft model. The mean EQV stresses of bilateral anterior alveolar arches, the maximum EQV stresses of maxilla and its alveolar arch on the cleft side in the model with bone graft in lower 1/3 of the alveolar cleft were significantly higher than those in full alveolar cleft bone graft model.

Conclusions: For UCCLP, bilateral maxillae, pterygoid processes of sphenoid bones and nasomaxillary, zygomaticomaxillary, pterygomaxillary sutures, anterior alveolar arch on the non-cleft side are the main occlusal load bearing structures before and after alveolar cleft bone graft. Alveolar cleft bone graft mainly affects biomechanical stabilities of nasal raphe and posterior alveolar arch, nasomaxillary suture on the non-cleft side. The areas near nasal floor and in the middle of the alveolar cleft are the key sites when bone grafting, and should be supplemented with bone graft when the bone resorbed in these areas.

Background

Based on epidemiological statistics, Nagase et al.[1] found UCCLP (Unilateral Complete Cleft Lip and Palate) to be the most prevalent type of cleft lip and palate. For patients with UCCLP, the two parts of the maxilla divided by the cleft are also different[2], the asymmetry of the nasomaxillary complexes[3–4] and the congenital sagittal asymmetric defect of the maxilla with collapsed bone segment deformity[5] on the cleft side are the common clinical manifestations. According to the summary by Janovica et al.[6], the occlusal forces of the dentition formed the specific bony conduction trajectories along the thickened buttresses of the maxillofacial bones, comprising a total of 7 vertical buttresses (bilateral nasomaxillary, zygomaticomaxillary, pterygomaxillary buttresses and the median sagittal buttress) and 3 horizontal buttresses (bilateral prefrontal, zygomatic and maxillary buttresses) to transmit the majority of occlusal

loads. The photoelastic technique also revealed that 3 main stress trajectories existed in the facial region, namely the nasomaxillary, zygomaticomaxillary and pterygomaxillary trajectories[7].The facial functional system was in the mechanical equilibrium between the dentition, muscles and bones[8], the instability of the maxillary segments caused by the maxillary buttress defect could lead to the secondary collapse and displacement of the maxilla[2]. On one hand, the cleft of the UCCLP can destroy the integrity of maxillofacial bone structures and interrupt the physiological occlusal stress transmission; on the other hand, the cleft is located on one side of the midline, the mechanical balance is lost and the stability of the maxillofacial structures will be affected, which in turn has a negative impact on the growth and development of the maxillofacial region. Harikrishnan et al.[9] and Zhao et al.[10] confirmed that the stress distribution between the cleft and non-cleft side of congenital unilateral maxilla cleft was asymmetrical and uneven through FEM(finite element method).

Bone graft in the cleft is the only method for alveolar cleft repairing currently. The most ideal alveolar cleft bone graft is full maxilla cleft bone graft, however, the shape of the cleft is extremely irregular, so it is difficult to achieve this goal, instead, the commonly used secondary full alveolar cleft bone graft is adopted in the clinic since it was reported by Boyne and Sands in 1972[11]. Yang et al.[12] had found that the stress-strain distribution became more symmetrical during maxilla anterior traction after alveolar cleft bone graft than before. Nagasao et al.[13] had applied uniform loads to the maxilla, alveolar and anterior side of the teeth to simulate upper lip pressure in UCCLP and found that the increased upper lip pressure exacerbated the facial asymmetry, which was alleviated by alveolar cleft bone graft. In summary, alveolar cleft bone graft can restore the integrity of bone segment, stabilize the bone segment and reconstruct the force conduction, distribute the stress of the maxilla cleft uniformly and alleviate the facial asymmetry.

Meanwhile, bone resorption after alveolar cleft bone graft is a common problem which has puzzled clinicians for a long time, the overall resorption rate was 10.4~100%[14–18]. The final effect of bone resorption after full alveolar cleft bone graft is almost always partial alveolar cleft bone graft, the surviving bones may be distributed in different sites of the alveolar cleft. Chen et al.[19] had studied the effect of maxilla anterior traction on the biomechanics of craniofacial bones of UCCLP after alveolar cleft bone graft and the grafted bone resorption by FEM, and found that the distribution of maxillofacial stresses and deformations was better when maxilla anterior traction was applied after bone graft, it was best in the non-resorbed and it was better in the resorbed when the lower part of the grafted bone than the upper part was lost. What's the effect of bones of different sites in the cleft on the maxillofacial biomechanical distributions of UCCLP under occlusal states? There's no report.

What is the effect of alveolar cleft bone graft on the maxillofacial biomechanical stabilities of UCCLP? From the view of maintaining the stabilities of maxillofacial biomechanics, which sites are the key regions of UCCLP should be ensured especially when grafting? Which sites should be supplemented with bone graft once bone resorption occurs even if the bones in other sites survive? In order to answer the clinical questions above, the research was carried out.

Results

Maxillofacial equivalent stress nephograms in non-bone graft model and models with bone graft in different sites of the alveolar cleft of UCCLP under four occlusal states (As in **Fig.1**. Since the overall strain nephograms of maxillofacial bone sutures were too large, so they cannot be presented in the article.)

Analysis indexes

Maxillofacial bones:

Equivalent (EQV) stress: Also known as von Mises stress. When an object is subjected to an external force, an internal force is generated within the object that resists the external force and restores the object from its post-deformation position to its pre-deformation position, the internal force per unit area at a point in its cross section is the stress. The von Mises stress reflects the stress state inside a structure by the stress contour, which can depict the stress variations in the structure after a load is applied.

Maxillofacial bone sutures:

EQV strain: The deformation per unit length of an object under stress is the strain. The total strain component is calculated by applying various types of loads to the object, then the EQV strain is calculated from the total deformation component. The type of EQV strain used in the research is elastic EQV strain.

The mean EQV stress or strain is the mean value of the EQV stresses or strains of the whole structure, which indicates the whole EQV stress or strain state of the structure; while the maximum EQV stress or strain is the maximum value of the EQV stresses or strains of the structure, which is located in a point on the structure and reflects the stress or strain concentration trend of the structure.

The statistical method

Three-way ANOVA was used to analyze the biomechanical data distribution variations of UCCLP maxillofacial structures with $P < 0.05$ as the statistical difference.

Biomechanical data distributions of UCCLP maxillofacial structures in non-bone graft model and models with bone graft in different sites of the alveolar cleft under four occlusal states (As in **Fig.2**, **3**)

Three-way ANOVA of biomechanical data distribution variations of UCCLP maxillofacial structures in non-bone graft model and models with bone graft in different sites of the alveolar cleft under four occlusal states (As in **Tab.1**, The biomechanical data type numbered A, B, C and D represented the mean

EQV stresses, maximum EQV stresses, mean EQV strains and maximum EQV strains respectively, the same as below.)

Tab.1

Three-way ANOVA of the biomechanical data distribution variations of UCCLP maxillofacial structures

Variable(Biomechanical data type)	Square Sum of Type III	Degree of Freedom	Mean Square	F	*P*
Models(A)	19.789	7	2.827	9.087	<0.001
Bones(A)	2865.586	13	220.43	708.587	<0.001
Occlusal states(A)	1414.802	3	471.601	1515.994	<0.001
Models * Bones(A)	129.153	91	1.419	4.562	<0.001
Models * Occlusal states(A)	15.324	21	0.73	2.346	0.001
Bones * Occlusal states(A)	1116.894	39	28.638	92.06	<0.001
Models(B)	850.863	7	121.552	9.724	<0.001
Bones(B)	272022.27	13	20924.79	1673.977	<0.001
Occlusal states(B)	41002.72	3	13667.573	1093.402	<0.001
Models * Bones(B)	3683.05	91	40.473	3.238	<0.001
Models * Occlusal states(B)	463.89	21	22.09	1.767	0.022
Bones * Occlusal states(B)	58329.084	39	1495.618	119.649	<0.001
Models(C)	0.003	7	0	3.338	0.002
Bone sutures(C)	0.87	8	0.109	984.689	<0.001
Occlusal states(C)	1.195	3	0.398	3607.877	<0.001
Models * Bone sutures(C)	0.011	56	0	1.739	0.004
Models * Occlusal states(C)	0.003	21	0	1.194	0.262
Bone sutures * Occlusal states(C)	1.097	24	0.046	413.78	<0.001
Models(D)	0.014	7	0.002	1.626	0.131
Bone sutures(D)	16.025	8	2.003	1580.179	<0.001
Occlusal states(D)	8.855	3	2.952	2328.323	<0.001
Models * Bone sutures(D)	0.118	56	0.002	1.665	0.007
Models * Occlusal states(D)	0.017	21	0.001	0.656	0.871
Bone sutures * Occlusal states(D)	10.295	24	0.429	338.393	<0.001

Simple effect analysis of biomechanical data distribution variations of the same UCCLP maxillofacial structure in different models under four occlusal states (As in **Tab.2** and **Fig.4**. Since the original table were too long, so only data with statistical significance, i.e. $P<0.05$ are presented in the article. The model

numbered 1 and 2, 3, 4, 5, 6, 7, 8 represents non-bone graft model and full maxilla cleft, full alveolar cleft, lower 2/3, upper 2/3, lower 1/3, middle 1/3, upper 1/3 bone graft model respectively.)

Tab.2

Simple effect analysis of biomechanical data distribution variations of the same structure

Structure (Biomechanical data type)		Square Sum	Degree of Freedom	Mean Square	F	*P*
CPS(A)	Contrast	5.197	7	0.742	2.387	0.022
	Error	84.926	273	0.311		
CA(A)	Contrast	117.89	7	16.841	54.138	<0.001
	Error	84.926	273	0.311		
NA(A)	Contrast	10.474	7	1.496	4.81	<0.001
	Error	84.926	273	0.311		
CP(B)	Contrast	785.5	7	112.214	8.977	<0.001
	Error	3412.513	273	12.5		
CA(B)	Contrast	2492.739	7	356.106	28.488	<0.001
	Error	3412.513	273	12.5		
CM(B)	Contrast	613.269	7	87.61	7.009	<0.001
	Error	3412.513	273	12.5		
NP(B)	Contrast	324.788	7	46.398	3.712	0.001
	Error	3412.513	273	12.5		
NR(C)	Contrast	0.002	7	0	2.419	0.022
	Error	0.019	168	0		
NNMS(C)	Contrast	0.006	7	0.001	7.201	<0.001
	Error	0.019	168	0		
NZTS(C)	Contrast	0.002	7	0	2.421	0.022
	Error	0.019	168	0		
NNMS(D)	Contrast	0.102	7	0.015	11.46	<0.001
	Error	0.213	168	0.001		

Tab.2, **Fig.4a-c** show that the mean EQV stresses of CPS, CA and NA were significantly different in different models(P<0.05).The mean EQV stresses of CPS were significantly higher in model 2 than in model 1(P<0.05), the mean EQV stresses of CA were significantly higher in model 6 than in other models(P<0.05), the mean EQV stresses of CA were significantly higher in model 4 than in model 1, 2, 5 and 8(P<0.05), the mean EQV stresses of CA were significantly higher in model 7 than in model 1(P<0.05), the mean EQV stresses of NA were significantly higher in model 6 than in model 2, 3 and 5 (P<0.05).

Tab.2, **Fig.4d-g** show that the maximum EQV stresses of CP, CA, CM and NP were significantly different in different models(P≦0.001).The maximum EQV stresses of CP were significantly higher in model 6 than in model 1, 2, 3, 5, 7 and 8 (P<0.05), the maximum EQV stresses of CA were significantly higher in model 6 than in other models (P<0.05), the maximum EQV stresses of CM were significantly higher in model 6 than in other models(P<0.05), the maximum EQV stresses of NP were significantly higher in model 1 than in model 2, 3 and 5(P<0.05).

Tab.2, **Fig.4h-j** show that the mean EQV strains of NR, NNMS and NZTS were significantly different in different models(P<0.05).The mean EQV strains of NR were significantly higher in model 1 than in model 3(P<0.05), the mean EQV strains of NNMS were significantly higher in model 1 than in other models (P<0.05), the mean EQV strains of NZTS were significantly higher in model 1 than in model 4 and 7(P<0.05).

Tab.2, **Fig.4k** show that the maximum EQV strains of NNMS were significantly different in different models(P<0.001).The maximum EQV strains of NNMS were significantly higher in model 1 than in other models (P<0.001).

Summaries of results

The main purpose of the research was to explore the effect of alveolar cleft bone graft on the UCCLP maxillofacial biomechanics, which sites should be supplemented with bone graft once bone resorption occurs. The most ideal alveolar cleft bone graft method-full maxilla cleft bone graft is difficult to achieve, so the commonly used full alveolar cleft bone graft is adopted. Therefore, the main comparative approach in the research was to use the biomechanical data of full alveolar cleft bone model as the standard, the biomechanical data of maxillofacial structures of models with bone graft in different sites of the alveolar cleft were compared with the standard.

The EQV stress distributions of UCCLP maxillofacial bones in different models under four occlusal states and the statistical analysis showed:

The mean and maximum EQV stresses of anterior alveolar arches on the non-cleft side, bilateral maxillae and pterygoid processes of sphenoid bones were all higher than other maxillofacial bones under the centric occlusion. The mean EQV stresses of pterygoid processes of sphenoid bones on the cleft side were all higher than other maxillofacial bones, the maximum EQV stresses of anterior alveolar arches on

the non-cleft side, maxillae and pterygoid processes of sphenoid bones on the cleft side were all higher than other maxillofacial bones under occlusion of the cleft side. The maximum EQV stresses of anterior alveolar arches on the non-cleft side were all higher than other maxillofacial bones under the anterior occlusion.

The maximum EQV stresses of posterior alveolar arch on the non-cleft side of full alveolar cleft bone graft model were significantly lower than non-bone graft model. The mean EQV stresses of bilateral anterior alveolar arches of lower 1/3 bone graft model were significantly higher than full alveolar cleft bone graft model, the maximum EQV stresses of maxilla and its alveolar arch on the cleft side of lower 1/3 bone graft model were significantly higher than full alveolar cleft bone graft model. There was no significant statistical difference in the EQV stress distributions of maxillofacial bone structures between full maxilla and full alveolar cleft bone graft model.

There was no significant difference in the EQV stress distributions of bilateral nasal bones, zygomata, temporal bones and maxillae, pterygoid processes of sphenoid bones on the non-cleft side of all models under four occlusal states. The EQV stresses of bilateral nasal bones and zygomata were generally lower than other maxillofacial bones.

The EQV strain distributions of UCCLP maxillofacial bone sutures in different models under four occlusal states and the statistical analysis showed:

The mean EQV strains of bilateral nasomaxillary, pterygomaxillary and zygomaticomaxillary sutures were all higher than other maxillofacial bone sutures, the maximum EQV strains of bilateral nasomaxillary sutures, pterygomaxillary sutures on the non-cleft side were all higher than other maxillofacial bone sutures under the centric occlusion. The mean and maximum EQV strains of ipsilateral nasomaxillary, pterygomaxillary and zygomaticomaxillary sutures were all higher than other maxillofacial bone sutures under occlusion of the cleft or the non-cleft side. The mean and maximum EQV strains of nasomaxillary sutures on the non-cleft side were all higher than other maxillofacial sutures under the anterior occlusion.

The mean EQV strains of nasal raphe and nasomaxillary suture on the non-cleft side of full alveolar cleft bone graft model were significantly lower than non-bone graft model, and the maximum EQV strains of nasomaxillary suture on the non-cleft side of full alveolar cleft bone graft model were significantly lower than non-bone graft model. There was no significant statistical difference in the EQV strain distributions between models with bone graft in other sites of the alveolar cleft and full alveolar cleft bone graft model.

There was no significant difference in the EQV strain distributions of bilateral pterygomaxillary, zygomaticomaxillary sutures and nasomaxillary, zygomaticote- mporal sutures on the cleft side of all models under four occlusal states.

Discussion

About 75% of patients with cleft lip and palate have varying degrees of alveolar cleft[20].There are asymmetrical bone movements in unilateral cleft lip and palate due to the special maxillofacial structure[21].Loss of bone and soft tissue on the cleft side and tension of the repaired lip on the non-cleft side can lead to flattening and recession of the central face[22]. Alveolar cleft bone graft is a key step of the sequential treatment for cleft lip/palate[23], a prominent function of it is stabilizing the maxillary dental arch to maintain dental stabilities and mastications[24], it can prevent re-collapse of the expanded maxillary segments[25].Therefore, alveolar cleft bone graft is of great significance for maxillofacial biomechanical stabilities.

Since the biomechanical properties of bone structures cannot be directly measured in the functional states in vivo at present, FEM has been greatly used in the field of oral and maxillofacial biomechanic researches[26].Through literature review[2, 9, 27–28],for the maxillofacial finite element modeling of cleft lip and palate, many scholars in the past tended to ignore the detailed structures such as periodontal membranes and bone sutures. However, the accuracy of the results mainly depended on the accuracy of the modeling process in finite element researches[29].After combining the results of stress magnitudes and directions, Viecilli et al.[30] concluded that the periodontal membrane was the initiating site of the force transmission, neglecting the presence of the periodontal membrane would lead to the inappropriate model simplification. Schmidt et al.[31] suggested a simplified modeling approach using uniform and consistent periodontal membrane layers, linear material properties for carrying out finite element researches to generate representative reference data, so the experiment integrated previous research outcomes and reconstructed periodontal membranes with 0.2mm thicknesses[32–33] on the root surfaces. As the joints of bones, the bone sutures could absorb and transmit transient mechanical stresses resulting from natural activities or applied actions externally[34]. In order to conform to the clinical reality as much as possible, the experiment was performed by dividing maxillofacial bones with reference to the original bone sutures. For the reconstruction of bone sutures, initially 0.5mm thick bone sutures were established in the junctions of bones according to the conclusion of Shi et al.[35]. However, the bone sutures appeared to be too wide to be realistic, so they were converted to 0.2mm widths which were more realistic and easier.

Bones can generate mechanical stresses due to physiological activities[36], they are mechanically and dynamically balanced[37].3D FEM is an effective method for studying complex craniofacial structures[38], which provides a complete description of the bone stress fields and is widely used to study bone mechanics[39]. FEM results are often shown in EQV stresses, i.e. von Mises stresses[29]. The von Mises principle, also known as the maximum deformation energy principle, is often used to estimate the yielding of ductile materials[29].von Mises stresses are mathematically calculated from components of compressive, shear and tensile stresses[40–41].Since von Mises stresses provide a clear depiction of the stress variations throughout the whole structure, it is a widely used EQV stress in biomechanical researches[42]. von Mises destruction theory has a certain amount of appropriateness and validity[29], it is one of the gold standards for evaluating bone stress distributions[43], therefore, EQV stresses were adopted as the indexes for analysis of maxillofacial bone biomechanical variations.

The craniofacial sutures have extremely complex forms[34], they are complex geometrical structures[44] and connective tissue connections between mineralized bones[45–46].They can transmit mechanical stresses and generate deformations [46].The abilities of bearing, absorbing and transmitting mechanical stresses are also inherent[34], and the abilities to conduct stresses between bones can be reflected in the deformations of bone sutures themselves. It is necessary to depict the biomechanical behaviors of human craniofacial sutures to understand the overall effects on load transmissions[47]. Reviewing the previous literature[5, 7, 8, 12, 19, 29, 45, 47–49], stresses were generally used as the analysis indexes of biomechanical variations in bone sutures. Mao et al.[34] and Zhang et al.[46] had studied the strains of the skull bone sutures under external forces and the bone sutures have a certain degree of movabilities[29]. So EQV strains were used as the analysis indexes of biomechanical variations in the maxillofacial bone sutures.

Gross et al.[50] found the strains increased on the alveolar arch and the nasal margin when simulated occlusal loads applied to the entire maxillary dental arch. Alexandridis et al.[7] found that stresses generated by occlusal loads were transmitted through maxilla along the nasal, zygomatic and pterygoid process pathways, in the zygomatic region, stresses were distributed posteriorly along the zygomatic arch to the temporal bone. Alexandridisi et al.[8] also found that in the midface, especially in the zygomatic region, the main effect of masseters on the zygomatic-temporal trajectory was very pronounced and most of the maxillary loads were borne by the region. It was also confirmed that the main stress trajectory of zygoma and zygomatic arch followed alveolar-maxillary-zygomatic-temporal bone direction, and the stresses were highly concentrated in the zygomatic process of temporal bone[8].The lateral maxilla was found to be the main vertical buttress in normal maxilla under maximum occlusal force by Pakdel et al.[51], the nasomaxillary buttress bore less loads, however there were insufficient evidences showed that the pterygomaxillary region to be a buttress structure.For UCCLP maxillofacial biomechanics, Zhao et al.[10] established a 3D maxilla finite element model with unilateral palatal cleft of a child as a specific object and initially analyzed the stress-strain distribution in the maxillary alveolar region under typical functional loads, it showed that the palatal deformity resulted in asymmetric stresses and strains distribution with higher stress and strain levels on the non-cleft side. Harikrishnan et al.[9] found that the normal cranium exhibited significant nasomaxillary, zygomaticomaxillary and pterygomaxillary buttress mechanic transfer trajectory actions under bilateral posterior occlusal loads by FEM. Whereas the role of nasomaxillary buttress was more pronounced on the cleft side than on the non-cleft side, the role of zygomaticomaxillary and pterygomaxillary buttress was more pronounced on the non-cleft side than on the cleft side in unilateral maxilla cleft under the same loads[9].

The results were in accordance with the conclusions of Gross et al.[50] and Pakdel et al.[51], it is evident that bilateral maxillae and their alveolar arches still played the roles of the center for occlusal load-bearing in UCCLP. The results showed that nasomaxillary and zygomaticomaxillary buttress of UCCLP did not play much strong occlusal load-bearing roles, whereas the role of the pterygomaxillary buttress was obvious, which differed significantly from the findings of Gross et al.[50] and Alexandridisi et al.[8], however, there were both similarities and differences with the findings of Pakdel et al.[51] and Harikrishnan et al[9]. The reason may be that pterygoid processes of sphenoid bones of UCCLP shared

more occlusal loads, thus the load-bearing roles of nasal bones and zygomata became weaken. From the data statistical analysis, it can be concluded that the area that be affected by alveolar cleft bone graft on the occlusal stress of UCCLP maxillofacial bones is mainly in the posterior alveolar arch on the non-cleft side. The results were also consistent with Chen et al.[19], and demonstrated that: Bone resorption near nasal base and in the middle of the alveolar cleft could significantly increase occlusal loads borne by bilateral anterior alveolar arches, it could also significantly enhance the concentration of occlusal stresses in the maxilla and its alveolar arch on the cleft side. However, the effect of resorption of the rest of the grafted bone in the alveolar cleft on the biomechanics of maxillofacial bones under occlusal loads was not significant.

Alexandridis et al.[7] found that occlusal stresses generated from closed-mouth muscles by mandible were concentrated on nasofrontal, zygomaticomaxillary and pterygopalatal suture, and in zygomatic region stresses were distributed upward to zygomaticofrontal suture and backward along the zygomatic arch to zygomaticotemporal suture. It is known from the results that nasomaxillary, pterygomaxillary and zygomaticomaxillary sutures of UCCLP are the main bone sutures bearing occlusal loads. It also confirms that occlusal loads can be transmitted along nasomaxillary, zygomaticomaxillary and pterygomaxillary buttresses through corresponding bone sutures. Alveolar cleft bone graft could significantly reduce occlusal loads borne by nasal raphe and nasomaxillary suture on the non-cleft side, and also significantly weaken the concentration of occlusal strains on nasomaxillary suture on the non-cleft side. It is demonstrated that alveolar cleft bone graft mainly affects the strain distribution of bone sutures above under occlusal loads. There were no significant differences in the EQV strain distributions on bilateral pterygomaxillary, zygomaticomaxillary sutures and nasomaxillary, zygomaticotemporal sutures on the cleft side before and after alveolar cleft bone graft, it is known that strains of the bone sutures above under corresponding occlusal loads are not affected by presence or absence of the grafted bone in the alveolar cleft.

It indicates from the results that alveolar cleft bone graft is necessary for UCCLP from maintaining the biomechanical equilibrium stability of maxillofacial bones, but there are insufficient biomechanical data to indicate the need for full maxilla cleft bone graft. Resorption of the grafted bone near nasal floor and in the middle of the alveolar cleft could significantly change biomechanical stabilities of maxilla and its alveolar arch on the cleft side as well as anterior alveolar arch on the non-cleft side, therefore, these areas are the sites that needed to be guaranteed when bone grafting, and supplementary bone graft should be performed when the grafted bone in these areas of the alveolar cleft resorbed. However, it must be noted that since human skulls have unique shapes and structures, the conclusions of stress-strain distributions derived from FEM can only be treated qualitatively but not quantitatively[52].

Conclusions

For UCCLP:

(1) Bilateral maxillae, pterygoid processes of sphenoid bones and bilateral nasomaxillary, zygomaticomaxillary, pterygomaxillary sutures and anterior alveolar arch on the non-cleft side are the main bearing structures for occlusal loads before and after alveolar cleft bone graft.

(2) Alveolar cleft bone graft mainly affects biomechanical stabilities of nasal raphe and posterior alveolar arch, nasomaxillary suture on the non-cleft side under occlusal loads.

(3) The areas near nasal floor and in the middle of the alveolar cleft are the sites that needed to be guaranteed when bone grafting, and supplementary bone graft should be performed when the grafted bone in these areas of the alveolar cleft resorbed.

Methods

Equipment and softwares

CT data acquisition equipment: Philips MX16-slice X-ray electron computed tomography device (Philips Electronics, Netherlands).

Softwares: Mimics 20 (Materialise, Belgium), Geomagic Studio 2014 (3D Systems, USA), Siemens PLM NX 12.0.0 (Siemens, Germany), ANSYS Workbench 19.2 (ANSYS, USA).

Materials

Equipment and softwares

CT data acquisition equipment: Philips MX16-slice X-ray electron computed tomography device (Philips Electronics, Netherlands).

Softwares: Mimics 20 (Materialise, Belgium), Geomagic Studio 2014 (3D Systems, USA), Siemens PLM NX 12.0.0 (Siemens, Germany), ANSYS Workbench 19.2 (ANSYS, USA).

Materials

A 24-year-old female typical UCCLP patient without skeletal systemic disorders, severe dropout of bone segments on both sides of the cleft and severe dentofacial plane deviation was selected. The patient's skull and neck were scanned by Philips MX 16-slice X-ray electron computed tomography device before alveolar cleft bone graft, the DICOM (Digital Imaging and Communications in Medicine) format data of CT were obtained. The use of the patient's CT data for the research was conducted with the patient's consent and approved by Medical Ethics Committee of West China Hospital of Stomatology, Sichuan University (Grant No. WCHSIRB-D-2020-362).

Establishment of UCCLP maxillofacial 3D CAD models of non-bone graft and bone graft in different sites of the alveolar cleft

The DICOM data were imported into Mimics, the cervical spines, hyoid bone and mandible with its dental images were removed, the model in .stl (StereoLithography) was generated as shown in Fig.5a, the microdontia was removed, the small holes were repaired, the surfaces of bones and teeth were trimmed. The model was then imported into Geomagic Studio, and further repaired, smoothed, finely modeled in planes and curved surfaces to obtain the model in .step (Standard for the Exchange of Product Model Data) , as shown in Fig.5b, the root surfaces of the maxillary teeth were expanded outward by 0.2 mm[32-33], the original alveolar sockets of the teeth were fitted to generate the periodontal ligaments of the tooth root surfaces by Boolean operations. The maxillary teeth, the periodontal ligaments and the craniomaxillofacial bone were imported into Siemens NX for assembly to obtain the 3D(Three-dimensional) CAD(Computer Aided Design)model in .prt, as shown in Fig.5c.

With the reference to bone sutures in the 3D CT reconstructed maxillofacial image, bones were depicted and segmented: CM (maxilla on the cleft side), CA (anterior alveolar arch on the cleft side), CP (posterior alveolar arch on the cleft side), CPS (pterygoid process of sphenoid bone on the cleft side), CN (nasal bone on the cleft side), CZ (zygoma on the cleft side), CT (temporal bone on the cleft side) and NM (maxilla on the non-cleft side), NA (anterior alveolar arch on the non-cleft side), NP (posterior alveolar arch on the non-cleft side), NPS (pterygoid process of sphenoid bone on the non-cleft side), NN (nasal bone on the non-cleft side), NZ (zygoma on the non-cleft side), NT (temporal bone on the non-cleft side). 0.2mm width bone sutures were depicted and reconstructed at the junctions of adjacent bones, the research mainly focused on bone sutures with maxilla buttress as the center: CNMS(nasomaxillary suture on the cleft side), CPMS (pterygomaxillary suture on the cleft side),CZMS (zygomaticomaxillary suture on the cleft side), CZTS (zygomaticotemporal suture on the cleft side), NR(Nasal Raphe), NNMS (nasomaxillary suture on the non-cleft side), NPMS (pterygomaxillary suture on the non-cleft side), NZMS (zygomaticomaxillary suture on the non-cleft side), NZTS (zygomaticotemporal suture on the non-cleft side).The cranial bones above the top of bilateral temporal bones were removed to obtain UCCLP maxillofacial CAD model in .prt, hereafter referred to as non-bone graft model, as shown in Fig.6a.

Non-bone graft model was imported into Semens NX to generate models of bone graft within full maxilla cleft (hereinafter referred to as full maxilla cleft bone graft model, as shown in Fig.6b) and full alveolar cleft bone graft model (hereinafter referred to as full alveolar cleft bone graft model, as shown in Fig.6c) respectively. The 3D CAD model of the grafted bone in the full alveolar cleft was divided into three equal parts according to the height with the nasal floor side as the upper surface and the alveolar ridge crest side as the lower surface. Comprehensively considering the possible bone resorption situations at different heights of the grafted bone after full alveolar cleft bone graft in the clinic, the middle 1/3 + lower 1/3, upper 1/3 + middle 1/3, lower 1/3, middle 1/3 and upper 1/3 part of the grafted bone in the full alveolar cleft were assembled with the original contact at two ends of the cleft respectively to form 5

models to simulate the rest grafted bone resorption, as shown in Fig.6d-h. The 5 models were hereafter referred to as lower 2/3, upper 2/3, lower 1/3, middle 1/3 and upper 1/3 bone graft model respectively, together with non-bone graft model, full maxilla cleft and full alveolar cleft bone graft model, they formed a total of 8 UCCLP maxillofacial CAD models of non-bone graft and bone graft in different sites of the alveolar cleft.

Different occlusal loads on UCCLP maxillofacial regions of the models

The occlusal plane was formed by the mesial contact point of the maxillary central incisors and the mesial buccal cusp apexes of bilateral first maxillary molars in Semens NX[28]. Models were imported into ANSYS Workbench, Young's moduli and Poisson's ratios of structures were set according to Tab. 3[49,53-54], the contact relationships of adjacent structures were set according to Tab.4. The imported models were tetrahedrally meshed. The occipital foramen magnum was set as the fixed constraint[42], the forces were loaded on the thrust surfaces of corresponding teeth, the directions of the loaded forces were perpendicular to the occlusal plane, the force values were set as in Tab.5[6].

Tab.3

Young's moduli and Poisson's ratios of structures

Structures	Young's modulus(MPa)	Poisson’s ratio
Craniomaxillofacial bones	13700	0.3
Grafted bone in the cleft	7900	0.3
Teeth	20000	0.3
Periodontal ligaments	0.49	0.49
Bone sutures	7	0.4

Tab.4

Contact relationships of adjacent structures

Adjacent structures	Contact relationships
Teeth and periodontal ligaments	Binding
Periodontal ligaments and maxilla	Binding
Bone sutures and peripheral bones	Binding
Grafted bone and the cleft	Fusion

Tab.5 Forces loaded on the maxillary dentition under four occlusal states

Tooth area / Force value(N) / Occlusal state	The cleft side			The non-cleft side		
	Anterior teeth area	Premolar area	Molar area	Anterior teeth area	Premolar area	Molar area
The centric occlusion	160	280	400	160	280	400
Occlusion of the cleft side	160	280	400	/	/	/
Occlusion of the non-cleft side	/	/	/	160	280	400
The anterior occlusion	160	/	/	160	/	/

Abbreviations

Abbreviation	Full name
UCCLP	Unilateral Complete Cleft Lip and Palate
FEM	Finite Element Method
EQV	Equivalent
DICOM	Digital Imaging and Communications in Medicine
.stl	StereoLithography
.step	Standard for the Exchange of Product Model Data
3D	Three-dimensional
CAD	Computer Aided Design

Declarations

Ethical Approval and Consent to participate

The research “Three-dimensional finite element analysis of the effect of alveolar cleft bone graft on the maxillofacial biomechanical stabilities of unilateral complete cleft lip and palate” was conducted with the participant’s consent and approved by Medical Ethics Committee of West China Hospital of Stomatology, Sichuan University (Grant No. WCHSIRB-D-2020-362).

Consent for publication:

All of the authors agree the article to be published in “Bio- Medical Engineering OnLine”.

Availability of supporting data:

All the data and materials of the research are availa- ble.

Competing interests:

There are no competing interests in the research.

Funding:

The research was supported by the clinical research project (Project approval No.: LCYJ 2019-10) of West China Hospital of Stomatology, Sichuan University.

Authors' contributions:

Tao Tian, Han-yao Huang, Bing Shi, Qian Zheng and Cheng-hao Li had proposed the conception and design; Tao Tian and Wei Wang had carried the experiment; Tao Tian, Cheng-hao Li had analysed and interpreted the data collected; Tao Tian had written the manuscript; Han-yao Huang, Bing Shi, Qian Zheng and Cheng-hao Li had revised the manuscript; Qian Zheng and Cheng-hao Li finally approved the manuscript.

Acknowledgements:

Many thanks for the time and consideration of dear staffs of “BioMedical Engineering OnLine” .

Authors' information:

The first author-Tao Tian:

Doctoral candidate, West China School of Stomatology, Sichuan University. E-mail: slonnierudiveckoal@163.com.

Han-yao Huang:

Lecturer, DDS, West China School of Stomatology, Sichuan University; West China Hospital of Stomatology, Sichuan University. E-mail: huanghanyao_cn@scu.edu.cn.

Wei Wang:

Engineer, Urumql DW Innovation InfoTech Co., Ltd. E-mail: wwind126@126.com.

Bing Shi:

Professor, DDS, West China School of Stomatology, Sichuan University; West China Hospital of Stomatology, Sichuan University. E-mail: shibingcn@vip.sina.com.

The corresponding Author 1-Qian Zheng:

Professor, DDS, West China School of Stomatology, Sichuan University; West China Hospital of Stomatology, Sichuan University. E-mail: zq652@163.com.

The corresponding Author 2-Cheng-hao Li:

Associate professor, DDS, West China School of Stomatology, Sichuan University; West China Hospital of Stomatology, Sichuan University. E-mail: leechenghao_cn@ 163.com.

References

1. Nagase Y, Natsume N, Kato T, Hayakawa T. Epidemiological Analysis of Cleft Lip and/or Palate by Cleft Pattern. J Maxillofac Oral Surg. 2010;9(4):389–95. https://doi.org/10.1007/s12663-010-0132-6.
2. Luo X, Huang H, Yin X, Shi B, Li J. Functional stability analyses of maxillofacial skeleton bearing cleft deformities. Sci Rep. 2019;9(1):4261–70. https://doi.org/10.1038/s41598-019-40478-w.
3. Laspos CP, Kyrkanides S, Tallents RH, Moss ME, Subtelny JD. Mandibular and maxillary asymmetry in individuals with unilateral cleft lip and palate. Cleft Palate Craniofac J.1997;34(3):232–9.https://doi.org/10.1597/1545-1569 _1997_034_0232_mamaii_2.3.co_2.
4. Suri S, Utreja A, Khandelwal N, Mago SK. Craniofacial computerized tomography analysis of the midface of patients with repaired complete unilateral cleft lip and palate. Am J Orthod Dentofacial Orthop. 2008;134(3):418-29. https://doi.org/10.1016/j.ajodo.2006.09.065.
5. Chen Z, Pan X, Zhao N, Shen G. Asymmetric maxillary protraction for unilateral cleft lip and palate patients using finite element analysis.J Craniofac Surg.2015;26(2):388–92.https://doi.org/10.1097/SCS.0000000000001337.

6. Janovic A, Saveljic I, Vukicevic A, Djuric M. Occlusal load distribution through the cortical and trabecular bone of the human mid-facial skeleton in natural dentition: a three-dimensional finite element study. Ann Anat. 2015;197:16–23. https://doi.org/10.1016/j.aanat.2014.09.002.
7. Alexandridis C, Caputo AA, Thanos CE. Distribution of stresses in the human skull.J Oral Rehabil. 1985;12(6):499-507.https://doi.org/ 10.1111/j.1365-2842. 1985.tb01297.x.
8. Alexandridis C, Thanos CE, Caputo AA. Distribution of stress patterns in the human zygomatic arch and bone. J Oral Rehabil. 1981;8(6):495–505. https:// doi.org/10.1111/j.1365-2842.1981.tb00524.x.
9. Harikrishnan P, Balakumaran V. Analysis of Stress Trajectories in Human Adult Cleft Skull. J Craniofac Surg. 2017;28(6):1552–3.https://doi.org/10. 1097/SCS.0000000000003849.
10. Zhao L, Patel PK, Harris GF, editors. Stress analysis of unilateral cleft palate using a three dimensional finite element model of pediatric subject-specific maxilla. Conf Proc IEEE Eng Med Biol Soc; 2004. https://doi.org/10.1109/IE MBS.2004.1404403.
11. Boyne PJ, Sands NR. Secondary bone grafting of residual alveolar and palatal clefts. J Oral Surg. 1972;30(2):87–92.
12. Yang IH, Chang YI, Kim TW, Ahn SJ, Lim WH, Lee NK, et al. Effects of cleft type, facemask anchorage method, and alveolar bone graft on maxillary protraction:a three-dimensional finite element analysis. Cleft Palate Craniofac J. 2012;49(2):221–9. https://doi.org/10.1597/10-265.
13. Nagasao T, Miyamoto J, Konno E, Ogata H, Nakajima T, Isshiki Y. Dynamic analysis of the effects of upper lip pressure on the asymmetry of the facial skeleton in patients with unilateral complete cleft lip and palate. Cleft Palate Craniofac J. 2009;46(2):154–60. https://doi.org/10.1597/07-177.1.
14. Tai CC, Sutherland IS. McFadden L.Prospective analysis of secondary alveolar bone grafting using computed tomography. J Oral Maxillofac Surg. 2000;58(11):1241–9. https://doi.org/10.1053/joms.2000.16623.
15. Van der Meij AJ, Baart JA, Prahl-Andersen B, Valk J, Kostense PJ, Tuinzing DB. Bone volume after secondary bone grafting in unilateral and bilateral clefts determined by computed tomography scans. Oral Surg Oral Med Oral Pathol Oral Radiol Endod.2001;92(2):136-41.https://doi.org/10.1067/moe. 2001.115274.
16. Feichtinger M, Mossböck R, Kärcher H. Assessment of bone resorption after secondary alveolar bone grafting using three-dimensional computed tomography: a three-year study. Cleft Palate Craniofac J. 2007;44(2):142–8. https://doi.org/10.1597/06-047.1.
17. Zhang W, Shen G, Wang X, Fan L. Evaluation of alveolar bone grafting using limited cone beam computed tomography. Oral Surg Oral Med Oral Pathol Oral Radiol. 2012;113(4):542–8. .https://doi.org/10.1016/j.oooo.2011.10.001.
18. Datana S, Chattopadhyay PK, Kadu A. Bony bridge resorption after secondary alveolar grafting and correlation with success of orthodontic treatment: A prospective volumetric cone beam computed tomography (CBCT) study. Med J Armed Forces India. 2019;75(4):375–82.https://doi.org/10.1016/j.mjafi. 2018.02.005.

19. Chen Z, Pan X, Shao Q, Chen Z. Biomechanical effects on maxillary protraction of the craniofacial skeleton with cleft lip and palate after alveolar bone graft. J Craniofac Surg.2013;24(2):446-53.https://doi.org/ 10.1097/ SCS. 0b013e31826cfe27.
20. Cho-Lee GY, Garcia-Diez EM, Nunes RA, Marti-Pages C, Sieira-Gil R, Rivera-Baro A. Review of secondary alveolar cleft repair. Ann Maxillofac Surg. 2013;3(1):46–50. https://doi.org/10.4103/2231-0746.110083.
21. Toscano D, Baciliero U, Gracco A, Siciliani G. Long-term stability of alveolar bone grafts in cleft palate patients. Am J Orthod Dentofacial Orthop. 2012;142(3):289–99. https://doi.org/10.1016/j.ajodo.2012.04.015.
22. Brauer RO, Cronin TD, Reaves EL. Early maxillary orthopedics, orthodontia and alveolar bone grafting in complete clefts of the palate. Plast Reconstr Surg Transplant Bull. 1962;29:625–41. .https://doi.org/10.1097/00006534-1962 06000–00001.
23. Xiao WL, Zhang DZ, Chen XJ, Yuan C, Xue LF. Osteogenesis effect of guided bone regeneration combined with alveolar cleft grafting: assessment by cone beam computed tomography. Int J Oral Maxillofac Surg. 2016;45(6):683-7. https://doi.org/10.1016/j.ijom.2016.01.013.
24. Waite PD, Waite DE. Bone grafting for the alveolar cleft defect. Semin Orthod. 1996;2(3):192–6. https://doi.org/10.1016/s1073-8746(96)80014-4.
25. Bajaj AK, Wongworawat AA, Punjabi A. Management of alveolar clefts. J Craniofac Surg. 2003;14(6):840. 6.https://doi.org/10.1097/00001665-2003110 00–00005.
26. Lisiak-Myszke M, Marciniak D, Bielinski M, Sobczak H, Garbacewicz L, Drogoszewska B. Application of Finite Element Analysis in Oral and Maxillofacial Surgery-A Literature Review. Materials (Basel). 2020;13(14):1–16. https://doi.org/10.3390/ma13143063.
27. Gautam P, Zhao L, Patel P. Biomechanical response of the maxillofacial skeleton to transpalatal orthopedic force in a unilateral palatal cleft. Angle Orthod. 2011;81(3):503–9. .https://doi.org/10.2319/070110-367.1.
28. Zhang D, Zheng L, Wang Q, Ma J. Displacements prediction from 3D finite element model of maxillary protraction with and without rapid maxillary expansion in a patient with unilateral cleft palate and alveolus. Biomed Eng Online. 2015;19:1–15. .https://doi.org/10.1186/s12938-015-0074-9.
29. Gautam P, Valiathan A, Adhikari R. Stress and displacement patterns in the craniofacial skeleton with rapid maxillary expansion: A finite element method study. Am J Orthod Dentofacial Orthop. 2007;132(1):5.e1-5.e11. https://doi. org/10.1016/j.ajodo.2006.09.044.
30. Viecilli RF, Katona TR, Chen J, Hartsfield JK Jr. Roberts WE.Three-dimensional mechanical environment of orthodontic tooth movement and root resorption. Am J Orthod Dentofacial Orthop. 2008;133(6):791 e11–26. https://doi.org/10.1016/j.ajodo.2007.11.023.
31. Schmidt F, Lapatki BG. Effect of variable periodontal ligament thickness and its non-linear material properties on the location of a tooth's centre of resistance.J Biomech. 2019;94:211-8.https://doi.org/10.1016/j.jbiomech. 2019. 07.043.

32. Coolidge DE. The thickness of the human periodontal membrane. J Am Dent Assoc. 1937;24:1260–70.
33. Gupta M, Madhok K, Kulshrestha R, Yadav A. Determination of stress distribution on periodontal ligament and alveolar bone by various tooth movements-A 3D FEM study. J Oral Biol Craniofac Res. 2020;10(4):758–63. https://doi.org/10.1016/j.jobcr.2020.10.011.
34. Mao JJ. Mechanobiology of craniofacial sutures.J. Dent Res. 2002;81(12):810–6. https://doi.org/10.1177/154405910208101203.
35. Shi Y, Zhu CN, Xie Z. Displacement and stress distribution of the maxilla under different surgical conditions in three typical models with bone-borne distraction: a three-dimensional finite element analysis. J Orofac Orthop. 2020;81(6):385–95. .https://doi.org/10.1007/s00056-020-00251-5.
36. Lindberg G, Banks-Sills L, Stahle P, Svensson I. A two-dimensional model for stress driven diffusion in bone tissue. Comput Methods Biomech Biomed Engin. 2015;18(5):457–67. .https://doi.org/10.1080/10255842.2013.807507.
37. Ben Kahla R, Barkaoui A, Merzouki T. Age-related mechanical strength evolution of trabecular bone under fatigue damage for both genders: Fracture risk evaluation. J Mech Behav Biomed Mater. 2018;84:64–73.https://doi.org/ 10.1016/j.jmbbm.2018.05.006.
38. Lee H, Ting K, Nelson M, Sun N, Sung SJ. Maxillary expansion in customized finite element method models. Am J Orthod Dentofacial Orthop. 2009;136(3):367–74. https://doi.org/10.1016/j.ajodo.2008.08.023.
39. Zannoni C, Mantovani R, Viceconti M. Material properties assignment to finite element models of bone structures: a new method. Med Eng Phys. 1998;20(10):735–40. https://doi.org/10.1016/s1350-4533(98)00081-2.
40. DeVocht JW, Goel VK, Zeitler DL, Lew D. A Study of the Control of Disc Movement Within the Temporomandibular Joint Using the Finite Element Technique.J Oral Maxillofac Surg.1996;54(12):1431–7.https://doi.org/ 10.101 6/s0278-2391(96)90259-1.
41. Gandy JR, Manuel CT, Leary RP, Wong BJ. Quantifying Optimal Columellar Strut Dimensions for Nasal Tip Stabilization After Rhinoplasty via Finite Element Analysis. JAMA Facial Plast Surg. 2016;18(3):194–200.https://doi. org/10.1001/jamafacial.2015.2261.
42. Wang M, Qu X, Cao M, Wang D, Zhang C. Biomechanical three-dimensional finite element analysis of prostheses retained with/without zygoma implants in maxillectomy patients. J Biomech. 2013;46(6):1155–61. https://doi.org/10. 1016/j.jbiomech.2013.01.004.
43. Yemineni BC, Mahendra J, Nasina J, Mahendra L, Shivasubramanian L, Perika SB. Evaluation of Maximum Principal Stress, Von Mises Stress, and Deformation on Surrounding Mandibular Bone During Insertion of an Implant:A Three-Dimensional Finite Element Study.Cureus.2020;12(7): e9430.https://doi.org/10.7759/cureus.9430.
44. Kopher RA, Mao JJ. Suture growth modulated by the oscillatory component of micromechanical strain. J Bone Miner Res. 2003;18(3):521–8. https://doi. org/10.1359/jbmr.2003.18.3.521.

45. Wang D, Cheng L, Wang C, Qian Y, Pan X. Biomechanical analysis of rapid maxillary expansion in the UCLP patient. Med Eng Phys. 2009;31(3):409–17. https://doi.org/10.1016/j.medengphy.2008.06.011.
46. Zhang ZQ, Yang JL. Biomechanical Dynamics of Cranial Sutures during Simulated Impulsive Loading. Appl Bionics Biomech. 2015;2015:596843. https://doi.org/10.1155/2015/596843.
47. Maloul A, Fialkov J, Wagner D, Whyne C. Characterization of craniofacial sutures using the finite element method. J Biomech. 2014;47(1):245–52. https://doi.org/10.1016/j.jbiomech.2013.09.009.
48. Olmez S, Dogan S, Pekedis M, Yildiz H. Biomechanical evaluation of sagittal maxillary internal distraction osteogenesis in unilateral cleft lip and palate patient and noncleft patients:a three-dimensional finite element analysis. Angle Orthod. 2014;84(5):815–24. .https://doi.org/10.2319/080613-586.1.
49. Yu HS, Baik HS, Sung SJ, Cho YS. Three-dimensional finite-element analysis of maxillary protraction with and without rapid palatal expansion. Eur J Orthod. 2007;29(2):118–25. .https://doi.org/10.1093/ejo/cjl057.
50. Gross MD, Arbel G, Hershkovitz I. Three-dimensional finite element analysis of the facial skeleton on simulated occlusal loading. J Oral Rehabil. 2001;28(7):684–94. https://doi.org/10.1046/j.1365-2842.2001.00711.x.
51. Pakdel AR, Whyne CM, Fialkov JA. Structural biomechanics of the craniomaxillofacial skeleton under maximal masticatory loading: Inferences and critical analysis based on a validated computational model. J Plast Reconstr Aesthet Surg. 2017;70(6):842–50. .https://doi.org/10.1016/j.bjps.2017.01.021.
52. Boryor A, Geiger M, Hohmann A, Wunderlich A, Sander C, Martin Sander F, et al. Stress distribution and displacement analysis during an intermaxillary disjunction—A three-dimensional FEM study of a human skull. J Biomech. 2008;41(2):376–82. .https://doi.org/10.1016/j.jbiomech.2007.08.016.
53. Tanaka E, Tanaka M, Watanabe M, Del Pozo R, Tanne K. Influences of occlusal and skeletal discrepancies on biomechanical environment in the TMJ during maximum clenching: an analytic approach with the finite element method. J Oral Rehabil. 2001;28(9):888–94. .https://doi.org/10.1046/j.1365-2842.2001.00763.x.
54. Jafari A, Shetty KS, Kumar M. Study of stress distribution and displacement of various craniofacial structures following application of transverse orthopedic forces–a three-dimensional FEM study.Angle Orthod. 2003;73 (1): 12-20.https://doi.org/10.1043/0003-3219(2003)073<0012:SOSDAD>2.0.CO; 2.

Figures

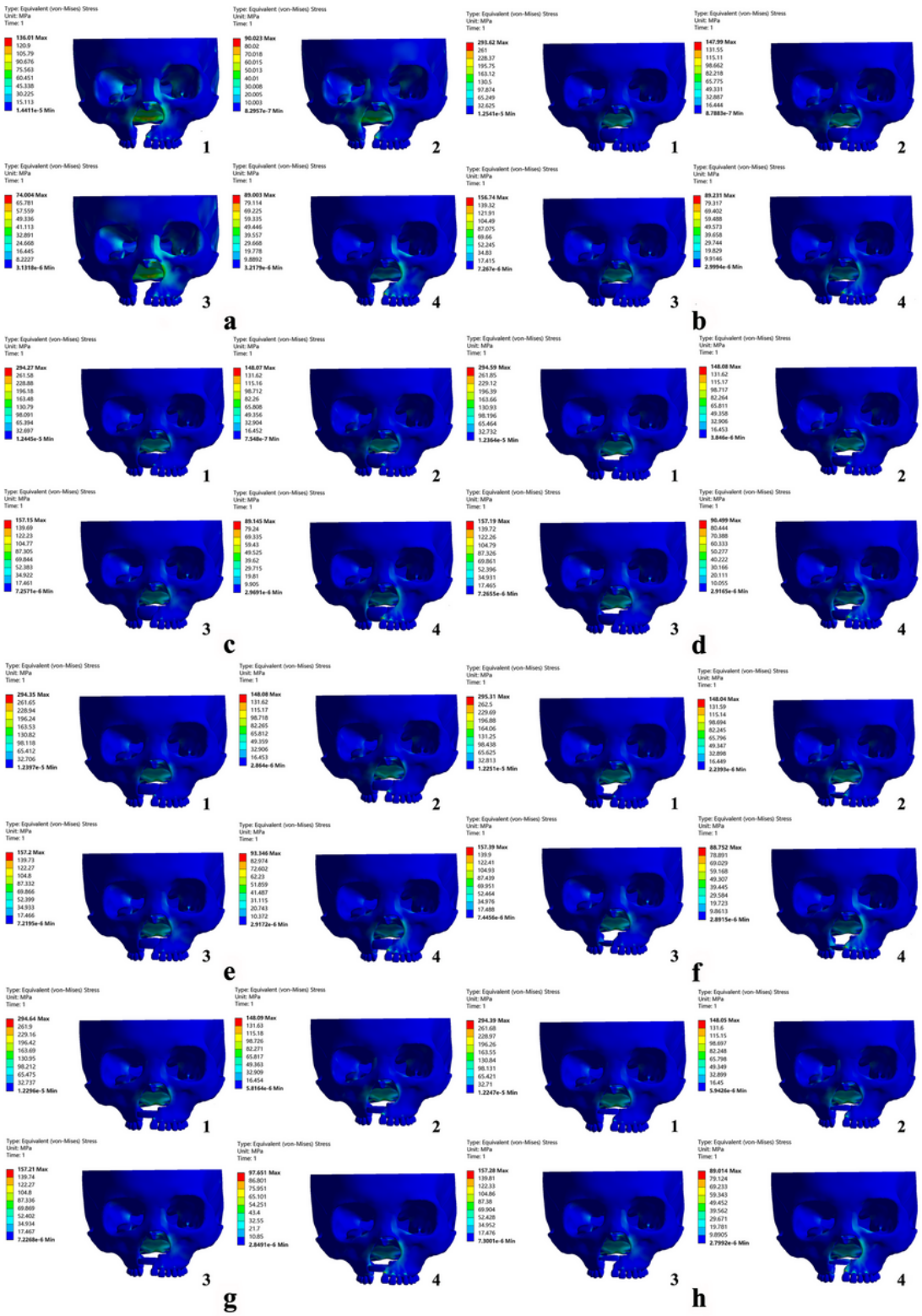

Figure 1

Equivalent stress nephograms of models under occlusal loads in ANSYS Workbench The sub-figures were represented respectively as: occlusion of the center (1), the cleft side (2), the non-cleft side (3) and the anterior teeth(4) on the maxillary dentition of non-bone graft(a), full maxilla cleft bone graft(b), full alveolar cleft bone graft(c), lower 2/3 bone graft(d), upper 2/3 bone graft(e), lower 1/3 bone graft(f), middle 1/3 bone graft(g) and upper 1/3 bone graft(h) model were simulated

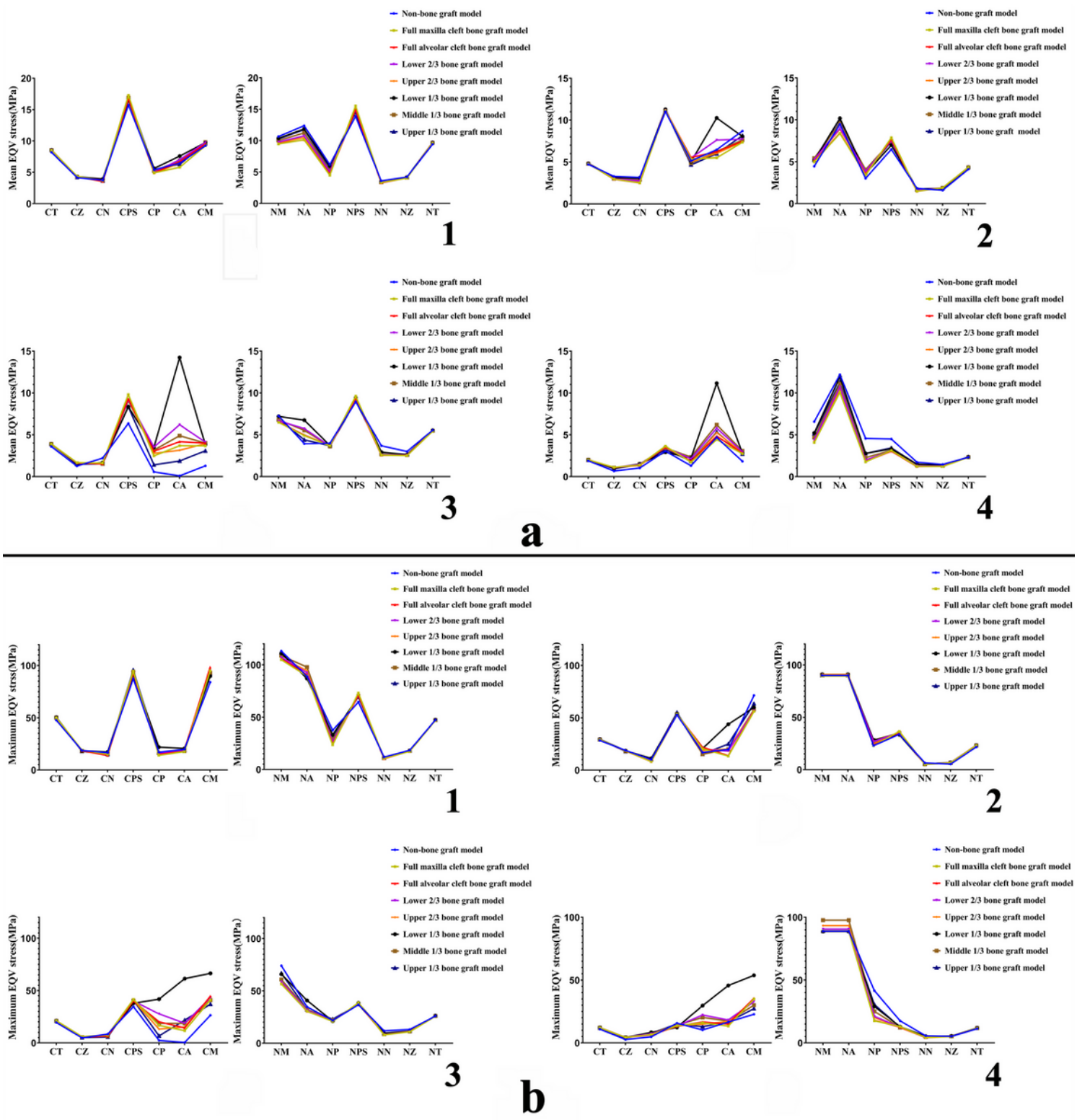

Figure 2

Mean and maximum EQV stress distributions of UCCLP maxillofacial bones Mean(a) and maximum(b) EQV stress distributions of maxillofacial bones in non-bone graft model and models with bone graft in different sites of the alveolar cleft under occlusion of the center(1), the cleft side(2), the non-cleft side(3) and the anterior teeth(4)

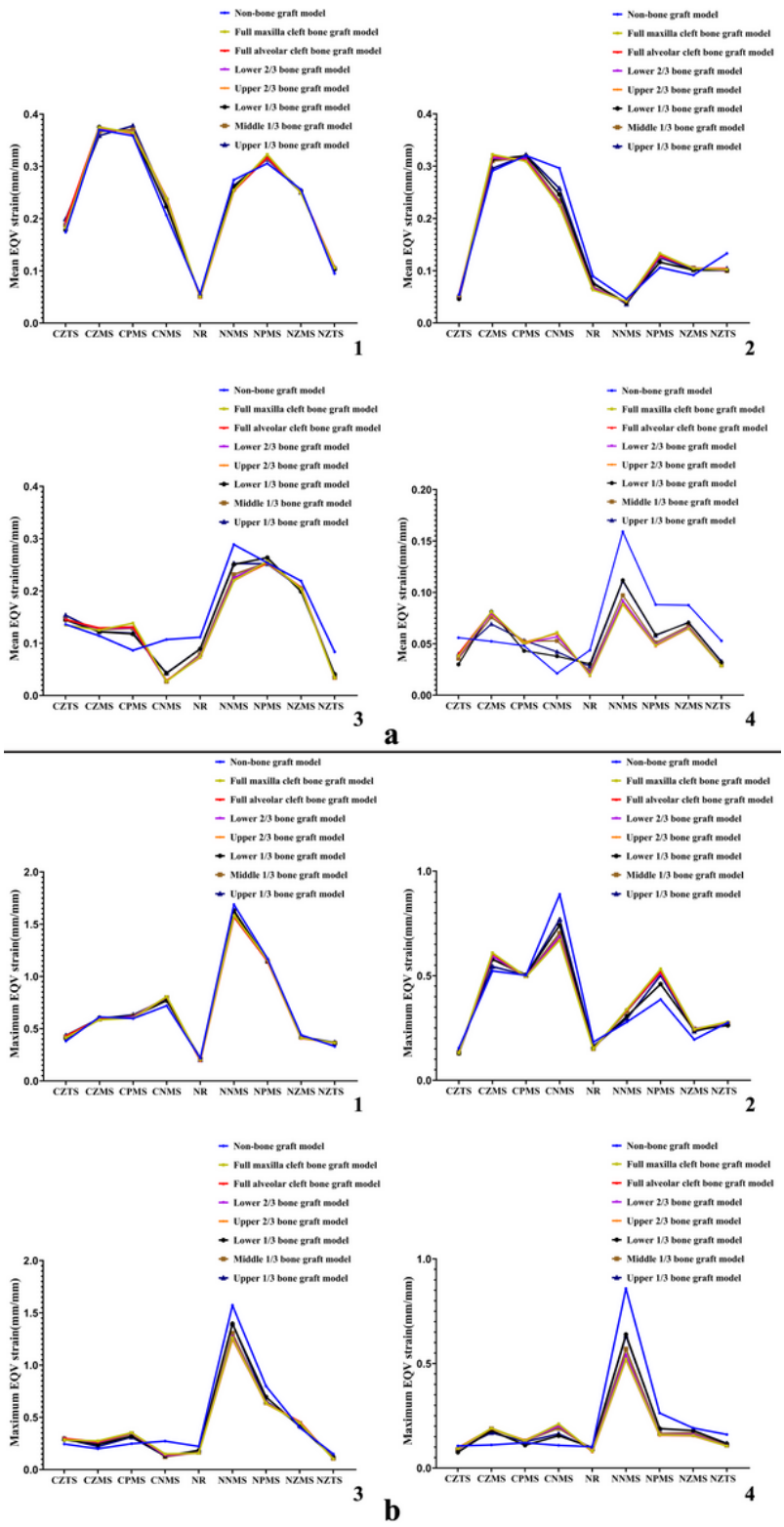

Figure 3

Mean and maximum EQV strain distributions of UCCLP maxillofacial bone sutures Mean(a) and maximum(b) EQV strain distributions of maxillofacial bone sutures in non-bone graft model and models with bone graft in different sites of the alveolar cleft under occlusion of the center(1), the cleft side(2), the non-cleft side (3) and the anterior teeth(4)

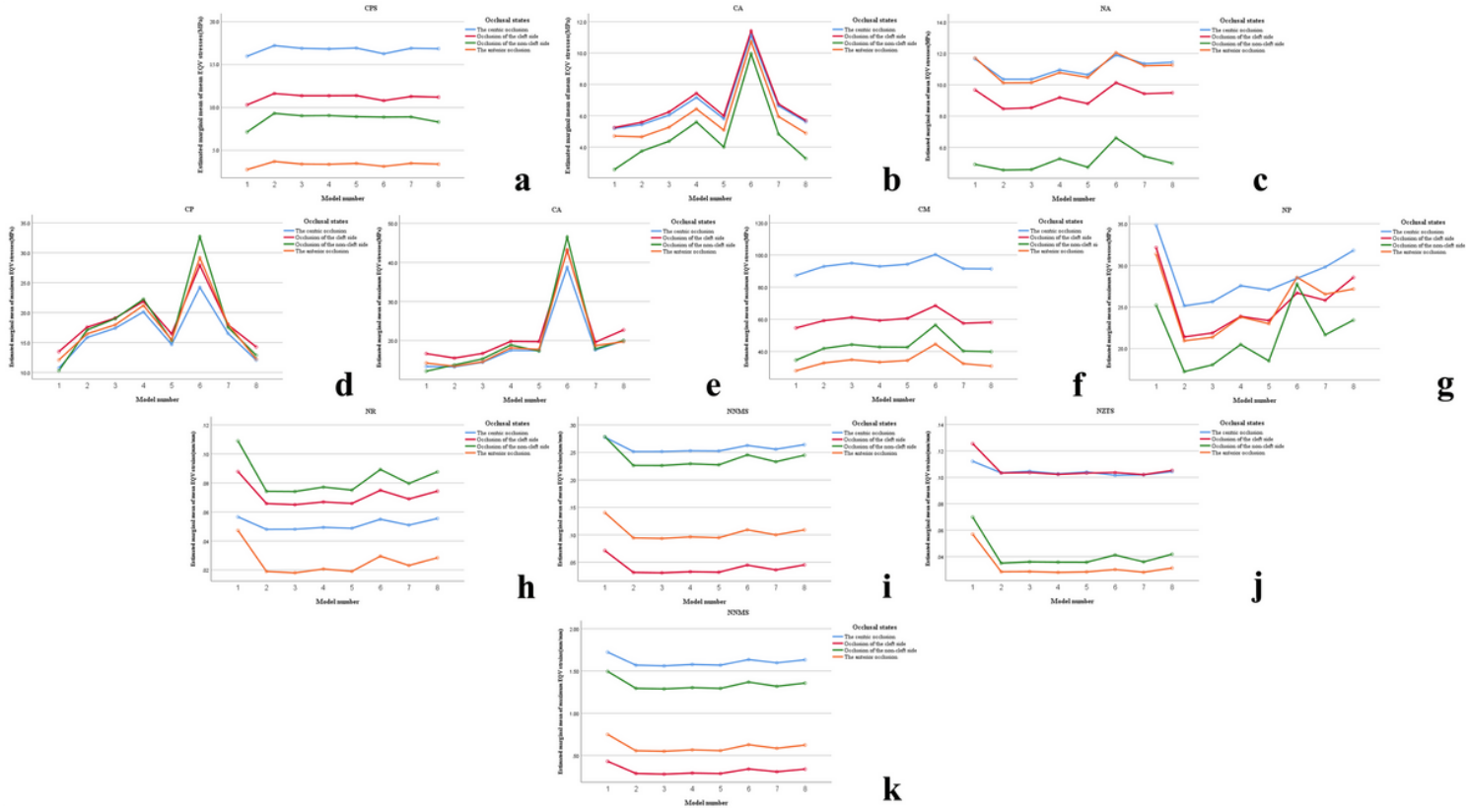

Figure 4

The estimated marginal mean diagrams of statistically significant structural biomechanical data In different models and under different occlusal states: Mean EQV stresses of CPS(a), CA(b) and NA(c); maximum EQV stresses of CP(d), CA(e), CM(f) and NP(g); mean EQV strains of NR(h), NNMS(i) and NZTS(j); maximum EQV strains of NNMS(k)

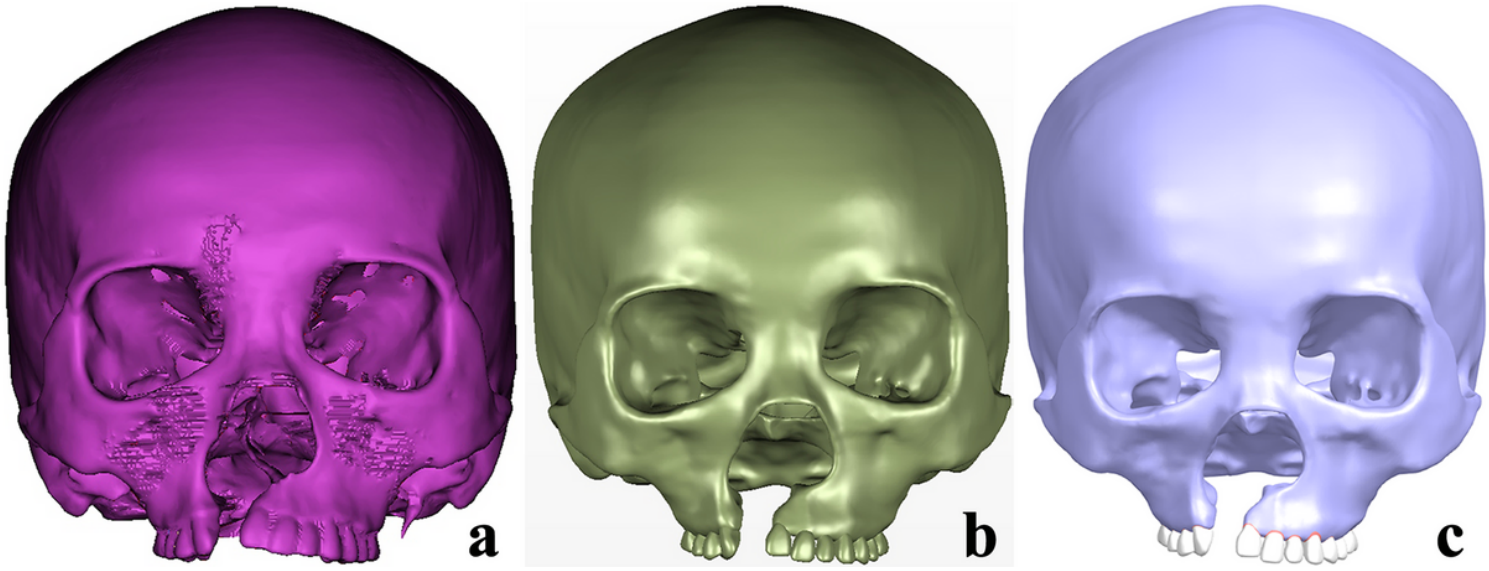

Figure 5

UCCLP craniomaxillofacial 3D CAD model a. the structural images not much relevant to the research were erased in Mimics, the model in .stl was obtained; b. the model in .step was obtained by further repairing, smoothing, finely modeling of planes and curved surfaces in Geomagic Studio; c. assembly of the maxillary teeth, the periodontal ligaments and the craniomaxillofacial bone in Siemens NX, the model in .prt was obtained

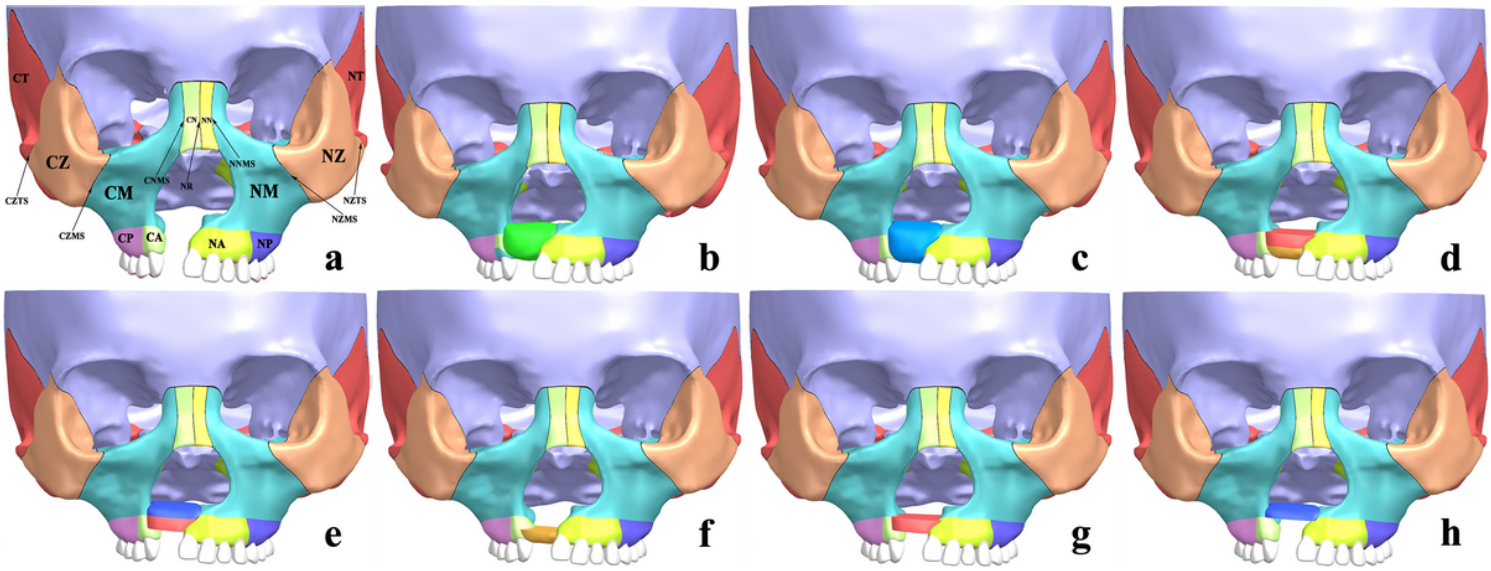

Figure 6

UCCLP maxillofacial 3D CAD models of non-bone graft and alveolar cleft bone graft Maxillofacial 3D CAD models of non-bone graft(a), full maxilla cleft(b) and full alveolar cleft(c) bone graft model, bone graft in lower 2/3 (d), upper 2/3 (e), lower 1/3 (f), middle 1/3 (g) and upper 1/3 (h) of the alveolar cleft according to the height with nasal floor as the upper surface and the alveolar ridge crest side as the lower surface

Supplementary Files

This is a list of supplementary files associated with this preprint. Click to download.

- Forcesloadedunderfourocclusalstates.png
- Tetrahedrallymeshing.png